World Academy of Science, Engineering and Technology
International Journal of Aerospace and Mechanical Engineering
Vol:2, No:11, 2008

Optimization of Kinematics for Birds and UAVs using Evolutionary Algorithms

Mohamed Hamdaoui, Jean-Baptiste Mouret, Stéphane Doncieux and Pierre Sagaut

***Abstract*—**The aim of this work is to present a multi-objective optimization method to find maximum efficiency kinematics for a flapping wing unmanned aerial vehicle. We restrained our study to rectangular wings with the same profile along the span and to harmonic dihedral motion. It is assumed that the birdlike aerial vehicle (whose span and surface area were fixed respectively to $1m$ and $0.15m^2$) is in horizontal mechanically balanced motion at fixed speed. We used two flight physics models to describe the vehicle aerodynamic performances, namely DeLaurier's model, which has been used in many studies dealing with flapping wings, and the model proposed by Dae-Kwan *et al*. Then, a constrained multi-objective optimization of the propulsive efficiency is performed using a recent evolutionary multi-objective algorithm called ϵ-MOEA. Firstly, we show that feasible solutions (i.e. solutions that fulfil the imposed constraints) can be obtained using Dae-Kwan *et al.*'s model. Secondly, we highlight that a single objective optimization approach (weighted sum method for example) can also give optimal solutions as good as the multi-objective one which nevertheless offers the advantage of directly generating the set of the best trade-offs. Finally, we show that the DeLaurier's model does not yield feasible solutions.

***Keywords*—**Flight physics, evolutionary algorithm, optimization, Pareto surface.

I. Introduction

NOWADAYS, UAVs (Unmanned aerial vehicles) are mainly used in the military field for observation and target destruction. People are also using them for civil applications like surveillance of road traffic, fire prevention, works of engineering inspection and more generally any intervention in dangerous or difficult to access places.

Recently, the research in this field has focused on a new dimension : the miniaturization. The goal is to conceive an autonomous flying vehicle small enough to be carried and operated by a single man. But this tendency is colliding with the performance problems encountered at low-Reynolds numbers. This has stimulated many scientists and engineers to consider non classical solutions. Some of them, inspired by nature, started to think of conceiving vehicles which fly like birds and insects by flapping their wings. Then, the concept of flapping wings UAVs appeared. This kind of UAVs has many advantages compared to the existing ones. Firstly, they can fly with suppleness at low-speed without the loss in performance which impacts fixed wings UAVs. Secondly, their acoustic signature is much more diffuse than the UAVs with rotating surfaces (helicopter-like UAVs), which makes them difficult to spot.

Among the prototypes developed in recent times, we can cite the entomopter of GeorgiaTech [19], Microbat of Caltech [14], Micromechanical flying insect [11] and the Project Ornithopter of DeLaurier [20], [16], [13]. In France, we can cite the PRF REMANTA [8], the ROBUR project [7] and the OVMI project [5].

Within each of these projects, the scientists tried to optimize the design of the aerial vehicle to increase its aerodynamic efficiency (lift, lift to drag ratio, power consumption, etc.). Actually, at the present time, an important part of the research and development community works on conceiving the most energy-efficient airfoil adaptation and wing motion technologies capable of providing the required aerodynamic performance for an UAV flight. We can refer to the recent work of Langelaan [4] dealing with trajectory optimization based on a simple flight physics model for soaring or the work of Zaeem *et al.* [6] about the design and optimization of a flapping wing mechanism for MAVs (Micro Air Vehicles). We can also cite the work of De Margerie *et al.* [3] that applies artificial evolution to optimize the morphology and kinematics of a flapping wing mini-UAV or the work of Berman *et al.* [1], where it is shown that the hovering kinematics for some insects minimize energy consumption. All of these works excepted De Margerie *et al.*'s, which does not make use of a tested model for flapping wings, use a single objective approach to solve the problem. In this work we focus our attention on kinematics optimization on a simple geometrical birdlike model (rectangular wings) in flapping motion (harmonic dihedral motion). This problem involves multiple objectives. We used an evolutionary algorithm to perform a multi-objective constrained optimization, demonstrated that there is a compatibility with the single objective approach (weighted sum method for example) and that the DeLaurier's model is not compatible with the optimization program.

Hamdaoui Mohamed is with the IJLRDA, University of Pierre et Marie Curie, Paris, email: hamdaoui@lmm.jussieu.fr
Jean-Baptiste Mouret is with ISIR, University of Pierre et Marie Curie, Paris, email: mouret@isir.fr
Stéphane Doncieux is with ISIR, University of Pierre et Marie Curie, Paris, email: Stéphane.Doncieux@isir.fr
Pierre Sagaut is with IJLRDA, University Pierre et Marie Curie, Paris, email: sagaut@lmm.jussieu.fr

II. Problem statement

We consider a simple birdlike model with rectangular wings of 1 meter span (both wings). We use a Liebeck LPT 110 A profile along the span. The flapping motion, considered as symmetric, can be decomposed into three basic motions, dihedral motion, sweep motion and twist motion also called pitch.

In our case, we are interested to consider only the dihedral

Fig. 1. The flapping motion can be decomposed into three basic motions : sweep, dihedral and twist

motion. The dihedral angle β is given by

$$\beta = d\beta cos(2\pi f_\beta t + \phi_\beta) \quad (1)$$

where $d\beta$, f_β, ϕ_β and t are respectively the amplitude of dihedral motion, the frequency of the dihedral motion, the phase of this motion and the time. Moreover we consider that the birdlike vehicle is in horizontal flight at a given velocity V_c.

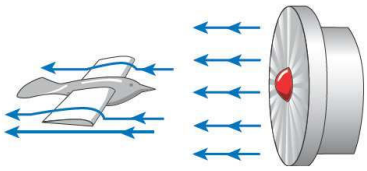

Fig. 2. The bird-like vehicle is in horizontal flight at a given speed

The motion of the wings can be decomposed into downstroke (downward motion of the wing) and upstroke (upward motion of the wing). The composition of this motion with the body motion (horizontal motion) gives a sinusoidal trajectory for the wingtips in an external referential as the motion of the wings is harmonic. The aerodynamic force exerted on the wings can be decomposed into lift and thrust. The surrounding fluid exerts also a drag force on the rest of the body.

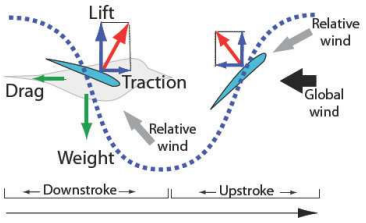

Fig. 3. The movement of the wings in an external referential

Many recent studies [18], [10], [22] have tried to identify and understand the high propulsive efficiencies encountered for example in nature (insects, birds, fishs) and others to find optimal designs maximizing the propulsive efficiency of UAVs [23], [22] .
It is the goal of this work to investigate a set of optimal kinematics that maximize propulsive efficiency in horizontal flight with prescribed velocity.

III. Materials and Methods

A. Flight physics models

The physics of the flapping flight is described by two flight physics models used separately.

1) The model of DeLaurier : Here is a description of DeLaurier's model. One can find all the necessary details about the original model in DeLaurier's paper [20]. DeLaurier presented an unsteady aerodynamic model for flapping wing flight based on a modified strip theory. Unsteady vortex-wake effects, partial leading edge suction and post stall behavior are accounted for as well as friction drag and camber.
Furthermore, this model assumes a continuous sinusoidal motion, with equal times between upstroke and downstroke, a high aspect ratio for the wing, an invariable finite span and a low resultant angle of attack.
The relevant variables for each section are presented as follows (Fig. 4) . For each section, the relative angle of attack (α) at the

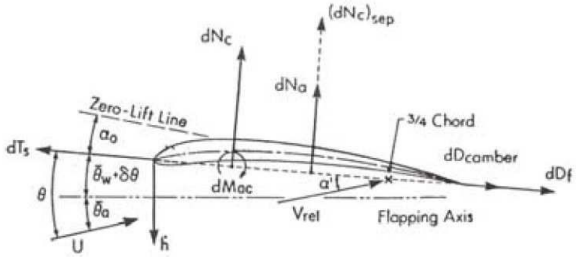

Fig. 4. Wing section aerodynamic forces and motion variables

$\frac{3}{4}$-chord location due to wing's motion and the flow's relative velocity (V) at $\frac{1}{4}$-chord location are given by :

$$\begin{aligned} \alpha &= \left[\frac{\dot{h}\cos(\theta-\bar{\theta_a}) + \frac{3}{4}c\dot{\theta} + U(\theta-\bar{\theta})}{U}\right], \\ V_x^2 &= \left[U\cos(\theta) - \dot{h}\sin(\theta-\bar{\theta_a})\right]^2, \\ V_n^2 &= \left[U(\alpha'+\bar{\theta}) - \frac{1}{2}c\dot{\theta}\right]^2, \\ V &= \sqrt{V_x^2+V_n^2}, \end{aligned}$$

with U the mean-stream velocity, $\dot{h}$ the plunging velocity (perpendicular to the flapping axis), θ the pitch angle, c the chord and $\bar{\theta} = \bar{\theta_w} + \bar{\theta_a}$ the mean pitch angle. Now assuming a sinusoidal motion, α' is given by

$$\alpha' = \frac{AR}{2+AR}\left[F'(k)\alpha + \frac{c}{2U}\frac{G'(k)}{k}\dot{\alpha}\right] - \frac{w_0}{U}, \quad (2)$$

with AR, the wing's aspect ratio, $\frac{w_0}{U}$ the downwash which can be approximated by $\frac{2(\alpha_0+\bar{\theta})}{2+AR}$, k the reduced frequency given

by $\frac{\omega c}{2U}$ (ω is the pulsation) and

$$\begin{aligned} F'(k) &= 1 - \frac{C_1 k^2}{(k^2 + C_2^2)}, \\ G'(k) &= -\frac{C_1 C_2}{(k^2 + C_2^2)}, \\ C_1 &= \frac{0.5AR}{(2.32 + AR)}, \\ C_2 &= 0.181 + \frac{0.772}{AR}. \end{aligned}$$

As the wing's aspect ratio is assumed to be large enough, the flow over each section is assumed to be chord-wise. Thus the section's circulatory force (dN_c) acting at $\frac{1}{4}$-chord location is given by

$$dN_c = \rho U V \pi(\alpha' + \alpha_0 + \bar{\theta}) c dy,$$

where ρ is the volumic mass of the fluid. An additional normal force (dN_a) acting at the mid-chord, due to apparent mass effect is given by

$$dN_a = \frac{\rho \pi c^2}{4} \dot{v_2} dy,$$

where $\dot{v_2} = U\dot{\alpha} - \frac{1}{4} c\ddot{\theta}$.
Therefore, the section's total attached flow normal force (dN) is

$$dN = dN_a + dN_c.$$

On the other hand, the chord-wise forces due to camber (dD_c), leading edge suction (dT_s) and friction drag (dD_f) are given by

$$\begin{aligned} dD_c &= -2\pi\alpha_0(\alpha' + \bar{\theta}) \frac{\rho U V}{2} c dy, \\ dT_s &= \eta_s 2\pi(\alpha' + \bar{\theta} - \frac{1}{4}\frac{c\dot{\theta}}{U})^2 \frac{\rho U V}{2} c dy, \\ dD_f &= (C_d)_f \frac{\rho V_x^2}{2} c dy, \end{aligned}$$

where $(C_d)_f$ is the friction drag coefficient (to be modeled against the Reynolds number). We adopted the same formula as DeLaurier which reads as follows $(C_d)_f = \frac{0.89}{[log(Re)]^{2.58}}$ with $Re = \frac{Vc}{\nu}$ the chord based Reynolds number with ν the kinematic viscosity of the surrounding air is $15\ 10^{-6} m^2.s^{-1}$. Thus, the total chord-wise force dF_x is

$$dF_x = dT_s - dD_c - dD_f.$$

Post stall behavior is locally modeled by using a stall criterion. The stall occurs when

$$\alpha' + \bar{\theta} - \frac{3}{4}(\frac{c\dot{\theta}}{U}) \geq (\alpha_{stall})_{max}. \quad (3)$$

where $(\alpha_{stall})_{max}$ is the static stall angle of incidence. Then it is assumed that all the chord-wise forces are zero ($dD_c, dT_s, dD_f = 0$) and the normal force (dN) is given by

$$\begin{aligned} dN &= (dN_c)_{sep} + (dN_a)_{sep}, \\ V_n &= \dot{h}\cos(\theta - \bar{\theta_a}) + \frac{1}{2}c\dot{\theta} + U\sin(\theta), \\ \widehat{V} &= (V_x^2 + V_n^2)^{\frac{1}{2}}, \\ (dN_c)_{sep} &= (C_d)_{cf} \frac{\rho \widehat{V} V_n}{2} c dy, \\ (dN_a)_{sep} &= \frac{1}{2} dN_a, \end{aligned}$$

with $(C_d)_{cf}$ the post stall normal force coefficient equal to 1.98.
The equations for vertical (dL) and horizontal (dT) forces are as follows :

$$\begin{aligned} dL &= dN\cos(\theta) + dF_x\sin(\theta), \\ dT &= dF_x\cos(\theta) - dN\sin(\theta). \end{aligned}$$

On integration along the span we get the vertical (L) and horizontal (T) forces

$$\begin{aligned} L &= 2\int_0^{\frac{b}{2}} \cos(\beta) dL, \\ T &= 2\int_0^{\frac{b}{2}} dD, \end{aligned}$$

with b the span (we consider the two wings). Then the averages are obtained by taking the mean in time over one period which gives

$$\begin{aligned} \bar{L} &= \frac{\omega}{2\pi}\int_0^{\frac{2\pi}{\omega}} L(t)\, dt, \\ \bar{T} &= \frac{\omega}{2\pi}\int_0^{\frac{2\pi}{\omega}} T(t)\, dt. \end{aligned}$$

It is worthwhile mentioning that one may also compute the instantaneous power required to move the section against its aerodynamic loads and the aerodynamic moment about the elastic axis. For attached flow one may note the following formulas :

$$\begin{aligned} dP_{in} &= dF_x \dot{h}\sin(\theta - \bar{\theta_a}) + dN\left[\dot{h}\cos(\theta - \bar{\theta_a}) + \frac{1}{4}c\dot{\theta}\right] \\ &+ dN_a\left[\frac{1}{4}c\dot{\theta}\right] - dM_{ac}\dot{\theta} - dM_a\dot{\theta}, \\ dM_{aero} &= dM_{ac} + dM_a - dN_a\left[\frac{1}{4}c - e\right] - dN_c\left[\frac{1}{2}c - e\right], \\ dM_{ac} &= \frac{1}{2}\rho U^2 C_{mac} c^2 dy, \\ dM_a &= -\left[\frac{1}{16}\rho\pi c^3\dot{\theta}U + \frac{1}{128}\rho\pi c^4\ddot{\theta}\right]. \end{aligned}$$

For stalled flow we have

$$\begin{aligned} (dP_{in})_{sep} &= dN_{sep}\left[\dot{h}\cos(\theta - \bar{\theta_a}) + \frac{1}{2}c\dot{\theta}\right], \\ (dM_{aero})_{sep} &= -((dN_c)_{sep} + (dN_a)_{sep})\left[\frac{1}{2}c - e\right], \end{aligned}$$

where e is the distance between the leading edge and the elastic axis (function of the span location). Similarly, we

can also derive expressions for the span integrated and time averaged moment about the elastic axis as follows

$$\begin{aligned}\bar{P}_{in} &= \frac{\omega}{2\pi}\int_0^{\frac{2\pi}{\omega}}\int_0^{\frac{b}{2}} dP_{in}\,dt,\\ \bar{M}_{aero} &= \frac{\omega}{2\pi}\int_0^{\frac{2\pi}{\omega}}\int_0^{\frac{b}{2}} dM_{aero}\,dt.\end{aligned}$$

Finally, we can define the average propulsive efficiency as follows

$$\bar{\eta} = \frac{\bar{T}U}{\bar{P}_{in}}.$$

2) The Dae-Kwan et al.'s model : Now we present the model of Dae-Kwan *et al.* as implemented within our code. This model is a modified version of DeLaurier's model for high angles of attack [2]. It includes a dynamic stall model. Moreover, it has been validated against experiments of oscillatory flat plate motion in pitch and plunge [2].
If we use the same notations as in section (III-A1) the model can be described as follows. The flow's relative velocity (V) at $\frac{1}{4}$-chord location for each section is given by :

$$\begin{aligned}V_x^2 &= \left[U\cos(\theta) - \dot{h}\sin(\theta-\bar{\theta_a})\right]^2,\\ V_n^2 &= \left[\dot{h}\cos(\theta-\bar{\theta_a}) - w_0 + \frac{1}{4}c\dot{\theta} + U\sin(\theta)\right]^2,\\ V &= \sqrt{V_x^2+V_n^2}.\end{aligned}$$

The angle of attack (γ) is given by

$$\gamma = \tan^{-1}\left[\frac{\dot{h}\cos(\theta-\bar{\theta_a}) + \frac{1}{4}c\dot{\theta} + U\sin(\theta) - w_0)}{U\cos(\theta) - \dot{h}\sin(\theta-\bar{\theta_a})}\right].$$

The linearized angle of attack ($\alpha'+\bar{\theta}$) at the $\frac{1}{4}$-chord location is given by

$$\begin{aligned}\alpha' &= \left[\frac{\dot{h}\cos(\theta-\bar{\theta_a}) + \frac{3}{4}c\dot{\theta} + U(\theta-\bar{\theta}) - w_0}{U}\right],\\ \alpha' &= \alpha - \frac{w_0}{U}.\end{aligned} \quad (4)$$

One can notice that V is not linearized, which was not the case in DeLaurier's model. Furthermore, there is no use of modified Theodorsen functions as can be seen from comparing equations (4) and (2).

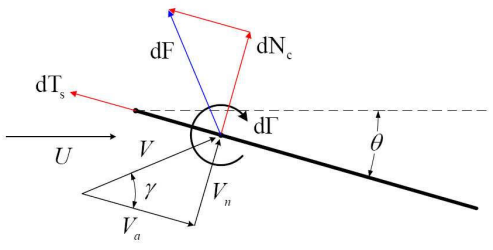

Fig. 5. The incidence correction adopted within Dae-Kwan *et al.* 's model

The section's representative vortex ($d\Gamma$) and the circulatory aerodynamic force (dF_c) are given by (Fig. 2) :

$$\begin{aligned}d\Gamma &= Uc\pi(\alpha'+\alpha_0+\bar{\theta}),\\ dF_c &= \rho V d\Gamma dy.\end{aligned}$$

Then the corrected form of the circulatory normal force (dN_c) is

$$dN_c = dF_c\cos(\gamma).$$

An additional normal force (dN_a) acting at the midchord, due to apparent mass effect is given by

$$dN_a = \frac{\rho\pi c^2}{4}\dot{v_2}dy,$$

where

$$\dot{v_2} = \ddot{h}\cos(\theta-\bar{\theta_a}) - \dot{h}\dot{\theta}\sin(\theta-\bar{\theta_a}) + \frac{1}{2}c\ddot{\theta} + U\dot{\theta}\cos(\theta).$$

Therefore the section's total attached flow normal force (dN) is

$$dN = dN_a + dN_c.$$

The chord-wise forces due to camber (dD_c), leading edge suction (dT_s) and friction drag (dD_f) are given by

$$\begin{aligned}dD_c &= -2\pi\alpha_0(\alpha'+\bar{\theta})\cos(\gamma)\frac{\rho UV}{2}cdy,\\ dD_f &= (C_d)_f\frac{\rho V_x^2}{2}cdy,\\ dT_s^1 &= (\alpha'+\bar{\theta}-\frac{1}{4}\frac{c\dot{\theta}}{U})\cos(\gamma),\\ dT_s^2 &= (\alpha'+\alpha_0+\bar{\theta})\sin(\gamma),\\ dT_s &= \eta_s 2\pi\left[(dT_s^1+dT_s^2)\frac{\rho UV}{2}cdy\right],\end{aligned}$$

where $V_x = U\cos(\theta) - \dot{h}\sin(\theta-\bar{\theta_a})$.
Thus, the total chord-wise force (dF_x) is

$$dF_x = dT_s - dD_c - dD_f.$$

The post stall behavior is locally modeled (for each section) by using a stall criterion. The stall occurs when

$$\gamma - \frac{3}{4}\left[\frac{c\dot{\theta}}{U}\right] \geq (\alpha_{stall})_{max},$$

which is the non linearized version of (3). Then it is assumed that $dD_c = 0$ and the other forces are given by

$$\begin{aligned}dN &= (dN_c)_{sep} + (dN_a)_{sep},\\ V_n &= \dot{h}\cos(\theta-\bar{\theta_a}) + \frac{1}{2}c\dot{\theta} + U\sin(\theta),\\ \widehat{V} &= (V_x^2+V_n^2)^{\frac{1}{2}},\\ (dN_c)_{sep} &= (C_d)_{cf}\frac{\rho\widehat{V}V_n}{2}cdy,\\ (dN_a)_{sep} &= \frac{1}{2}dN_a,\\ (dD_f)_{sep} &= (C_d)_f^{stall}\frac{\rho V_x^2}{2}cdy,\\ (dT_s)_{sep} &= \eta_s^{stall}2\pi(\alpha'+\bar{\theta}-\frac{1}{4}\frac{c\dot{\theta}}{U})\cos(\gamma)\frac{\rho UV}{2}cdy,\end{aligned}$$

$(dT_s)_{sep}$ accounts for the dynamic stall phenomena and contributes to the normal force (dN) (Fig. 3).

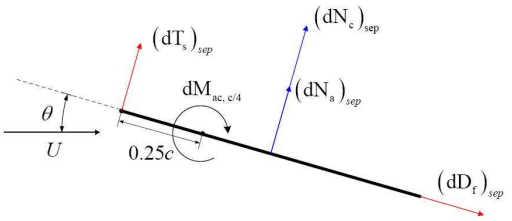

Fig. 6. The modelisation of dynamic stall within Dae-Kwan *et al.*'s model

The constants η_s^{stall} and $(C_d)_f^{stall}$ were taken equal respectively to 1.491 and 0.065. Now we can derive the equations for vertical (dL) and horizontal (dT) forces as follows :

$$\begin{aligned} dL &= dN\cos(\theta) + dF_x\sin(\theta), \\ dT &= dF_x\cos(\theta) - dN\sin(\theta). \end{aligned}$$

On integration along the span we get the vertical (L) and horizontal (T) forces

$$\begin{aligned} L &= 2\int_0^{\frac{b}{2}} \cos(\beta) dL, \\ T &= 2\int_0^{\frac{b}{2}} dD, \end{aligned}$$

with β the dihedral angle which is a function of time and b the span (we consider both wings).
Then the averages are obtained by taking the mean in time over one period which gives

$$\begin{aligned} \bar{L} &= \frac{\omega}{2\pi}\int_0^{\frac{2\pi}{\omega}} L(t)dt, \\ \bar{T} &= \frac{\omega}{2\pi}\int_0^{\frac{2\pi}{\omega}} T(t)dt. \end{aligned}$$

One may also compute the instantaneous power required to move the section against its aerodynamic loads and the aerodynamic moment about the elastic axis. For attached flow it is given by

$$\begin{aligned} dP_{in} &= dF_x\dot{h}\sin(\theta-\bar{\theta_a}) + dN\left[\dot{h}\cos(\theta-\bar{\theta_a}) + \frac{1}{4}c\dot{\theta}\right] \\ &+ dN_a\left[\frac{1}{4}c\dot{\theta}\right] - dM_{ac}\dot{\theta} - dMa_a\dot{\theta}, \\ dM_{aero} &= dM_{ac} + dM_a - dN_a\left[\frac{1}{4}c - e\right] - dN_c\left[\frac{1}{2}c - e\right], \\ dM_{ac} &= \frac{1}{2}\rho U^2 C_{mac} c^2 dy, \\ dM_a &= -\left[\frac{1}{16}\rho\pi c^3\dot{\theta}U + \frac{1}{128}\rho\pi c^4\ddot{\theta}\right]. \end{aligned}$$

For stalled flow we have

$$\begin{aligned} (dP_{in})_{sep} &= dN_{sep}\left[\dot{h}\cos(\theta-\bar{\theta_a}) + \frac{1}{2}c\dot{\theta}\right], \\ (dM_{aero})_{sep} &= -\left[(dN_c)_{sep} + (dN_a)_{sep}\right]\left[\frac{1}{2}c - e\right], \end{aligned}$$

with e the distance between the leading edge and the elastic axis. It is clear that e is a function of the span location. We can also derive expressions for the span integrated and time averaged moment about the elastic axis as follows

$$\begin{aligned} \bar{P}_{in} &= \frac{\omega}{2\pi}\int_0^{\frac{2\pi}{\omega}}\int_0^{\frac{b}{2}} dP_{in}\, dt, \\ \bar{M}_{aero} &= \frac{\omega}{2\pi}\int_0^{\frac{2\pi}{\omega}}\int_0^{\frac{b}{2}} dM_{aero}\, dt. \end{aligned}$$

Finally we can define the average propulsive efficiency as follows

$$\bar{\eta} = \frac{\bar{T}U}{\bar{P}_{in}}.$$

B. Optimization : concepts and tools

1) Terminology : When dealing with an optimization problem, specific vocabulary is used. On its most general form a multi-objective optimization problem reads as follows

$$\begin{aligned} max \quad & f_m(x) \quad , m = 1...M, \\ g_j \quad & \geq \quad 0, \, j = 1...K, \\ h_j \quad & = \quad 0, \, j = 1...L, \\ x_i^l \leq \quad & x_i \quad \leq x_i^u, \, i = 1...n, \end{aligned} \tag{5}$$

where M is the number of objectives, K the number of inequality constraints (represented by the functions g_j) and L the number of equality constraints (represented by the functions h_j).
The vector $x = (x_1, ..., x_n)$ is the n decision variables vector. The n numbers x_i^l and x_i^u are respectively the lower and upper bounds of the variable x_i. These bounds define the *search space* or *decision space*, **D**. What is commonly called solution is an element of the decison space. A solution will be feasible if it satisfies the constraints. The group of feasible solutions is called the *feasible space*, **S**.

2) Dominance and Pareto optimality : A solution x^i of the problem (5) is said to dominate another solution x^j, if the following conditions are satisfied :

- The solution x^i is not worse than x^j with respect to all objectives which means that $f_m(x^i) \geq f_m(x^j) \quad \forall m \in \{1...M\}$.
- The solution x^i is strictly better than x^j with respect to at least one objective which means that $\exists m \in \{1...M\}$ such that $f_m(x^i) > f_m(x^j)$

The *global Pareto set* of the multi-objective optimization problem (5) is composed of the feasible solutions that are not dominated by any other solution of the feasible space. The image of the Pareto set in the objectives' space is called *Pareto surface* or *Pareto front* for a bi-objective problem (Fig. 7).

3) Search procedures of the non-dominated set : Most optimization problems involve numerous objectives in practice. The standard approach is to transform them into a single-objective by using a weighted sum of the relevant objectives as follows (6) :

$$F_w(x) = \sum_{m=1}^{M} w_m f_m(x), \tag{6}$$

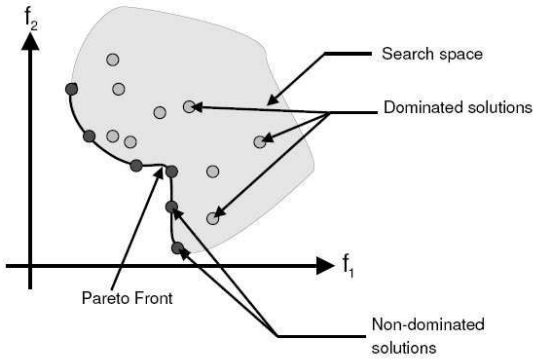

Fig. 7. Pareto front, dominated and non dominated solutions

where the weights $w_m \geq 0$ verify $\sum_{m=1}^{M} w_m = 1$. Then, to solve the problem (5), the following optimization program is resolved :

$$max_{\,x \in \mathbf{S}} F_w(x). \tag{7}$$

The solution of the problem (7) is included in the Pareto surface. It is given by the tangency points between the Pareto surface and the hyperplan whose normal is the vector $w = (w_1, ..., w_M)$. Then by changing the values of the weights we can get the whole front if it is convex [15].

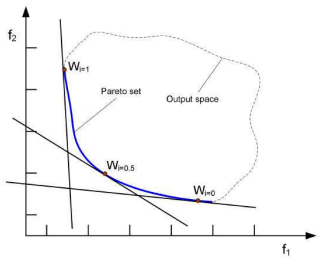

Fig. 8. Example of three different solutions obtained in the case of three different weighted sums with a convex Pareto front

If the Pareto surface is an hyperplan in the objectives' space then the two approaches are equivalent and one will prefer the single-objective approach for its simplicity. But if the Pareto surface is concave, or changes curvature then the single-objective method will be unable to get all the Pareto surface points by changing the weights [15].
On the contrary, multiobjective optimization procedures produce a set of trade-offs, among which a higher-level algorithm, or the user, may select the preferred one without the need to a priori assign relative weights to these alternatives. One of the most interesting properties of evolutionary optimization methods is their ability to deal with multiple objectives at once. Numerous algorithms have been proposed [12], to generate the set of such trade-offs. Most of them rely on the concept of domination and generate the so-called Pareto surface.
In this work to generate globally Pareto-optimal sets we used the ϵ-MOEA algorithm [9] for its efficiency and robustness. It is based on the ϵ-dominance concept, where ϵ controls the allowable difference between two values of the vector of objective functions, it may be considered as the resolution in the objectives' space. Moreover it is a steady state MOEA (Multi Objective Evolutionary Algorithm), that emphasizes non-dominated solutions by using an elitist approach.

4) Optimization program : To begin with, we need to state some relevant variables for our problem. In horizontal flight, with symmetrical flapping motion and prescribed forward velocity we have the following equalities :

$$\begin{aligned} L &= W, & (8)\\ D &= T, & (9)\\ M &= 0, \end{aligned}$$

where L is the lift, W is the weight, T is the thrust, D the body drag and M the pitching moment about the elastic axis of the wing. These are the equations to satisfy in this case.

Following empirical relations established for birds [17], we compute an average mass M ($0.69\ kg$) for the whole device (wings+fuselage+appendages+equipments) and an average surface area S of the wings ($0.15m^2$). Provided (8), this allows us to determine the necessary lift coefficient C_{zc} to ensure sustentation for a given cruise velocity as follows :

$$C_{zc} = \frac{2Mg}{\rho S V_c^2},$$

where g ($10.0\ m.s^{-2}$) is the acceleration of gravity and ρ ($1.295\ kg.m^{-3}$) is the volumic mass of air. One can find the values of C_{zc} in table (IV). The empirical relations provided by [17], allow us to estimate maximum and minimum values for mass (M_{max} and M_{min}) and cruise velocity (V_{max} and V_{min}) for a birdlike vehicle with the prescribed span. Then, using (8), we can determine maximum (C_{zmax}) and minimum (C_{zmin}) values for the mean lift coefficient.

With an estimation for birds of the mean body drag (C_{dc}) [17], we can compute also maximum (C_{dmax}) and minimum (C_{dmin}) values for the drag coefficient. Provided (9), this gives us upper and lower bounds for the mean thrust coefficient C_T as well. One can find the values of mass and frequencies in table (I) and the values of aerodynamical parameters in (II).

Now, we are ready to deal with the optimization part. The optimization variables are the kinematical parameters of the dihedral motion given in (1). Then, we have

$$\begin{aligned} x_1 &= d\beta,\\ x_2 &= f_\beta,\\ x_3 &= \phi_\beta. \end{aligned}$$

The upper and lower bounds for the optimization variables are defined as follows

$$\begin{aligned} x^u &= (\frac{\pi}{2}, f_{max}, \pi),\\ x^l &= (-\frac{\pi}{2}, f_{min}, -\pi). \end{aligned}$$

One can find all the relevant values for x^u and x^l in table (III).
We define then the following optimization program, called (OP) which involves three objectives :

- Maximise the propulsive efficiency with $C_{din} \leq C_T \leq C_{dmax}$,
- Minimize the distance between the lift coefficient C_z and C_{zc} with
  1) $C_{zmin} \leq C_z \leq C_{zmax}$,
  2) $\frac{M_{min}-M}{M} \leq \frac{C_z-C_{zc}}{C_{zc}} \leq \frac{M_{max}-M}{M}$,
- Minimize the absolute value of the pitch moment coefficient C_m.

5) The optimisation code : We used for optimization an open source code, Sferes (Framework Enabling Research on Evolution and Simulation) written in C++, developed by Samuel Landau and Stéphane Doncieux [25]. It is a tool dedicated to students, searchers or others interested in the evolutionary algorithm experiments. Its goal is to provide a generic tool maximizing code reuse and thus accelerating the development of new algorithms by concentrating on the new aspects. Moreover Sferes gathers an evolution framework with a simulation framework. It can be used for multi or single objective optimization. We implemented within the code a module providing the value of the objectives and constraints using the model of DeLaurier's and Dae-Kwang *et al.*'s model.

IV. Results and discussion

A. General considerations

We solve the problem (OP) using Dae-Kwan *et al.*'s model and the DeLaurier's model with the bounds for optimization parameters specified in table (III). We used an asymmetrical function (Fig. 9), defined as follows, to scale our objectives.

$$\psi = \begin{cases} \frac{1}{x+1} & \text{if } x > 0, \\ \frac{-1}{x-1} - 1 & \text{otherwise.} \end{cases}$$

This function was used to favour finding positive values of x, which in our case (see (OP)) means finding propulsive efficiencies ($\bar{\eta}$) as close to 1.0 as possible, lift coefficients (C_z) slightly superior to the targeted lift coefficient (C_{zc}) and pitching moment coefficients (C_m) slightly superior to zero. We have penalized each criteria with a penalty function Π

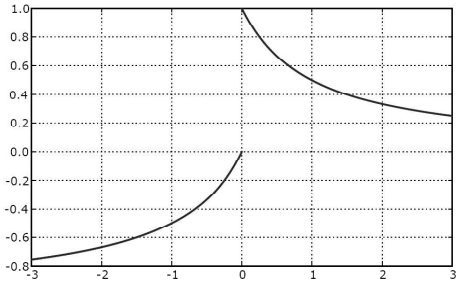

Fig. 9. Function $y = \psi(x)$ used to scale the objectives

using the Heaviside function H usually defined by

$$H(x) = \begin{cases} 1 & \text{if } x > 0, \\ 0 & \text{otherwise.} \end{cases}$$

The penalty function is defined as follows

$$\begin{aligned} \Pi \;=\; & -H(\bar{\eta}-1) - H(-\bar{\eta}), \\ & -H(C_T - C_{dmax}), \\ & -H(C_{dmin} - C_T), \\ & -H(C_z - C_{zmax}) - H(C_{zmin} - C_z). \end{aligned}$$

We have not included in the penalty function the constraint on $\frac{C_z-C_{zc}}{C_{zc}}$ but we will take it into account by eliminating the provided solutions that do not respect this constraint to finally obtain the feasible set. Therefore the optimized objectives are as follows:

- Maximize $F_1 = \psi(\bar{\eta}-1) + 2\Pi - 2$,
- Maximize $F_2 = \psi(C_z - C_{zc}) + 2\Pi - 2$,
- Maximize $F_3 = \psi(C_m) + 2\Pi - 2$.

We can notice that when the penalty is zero, the objectives take values between -3.0 and -1.0, but if the penalty is not zero then the objectives will take values inferior to -3.0. Then solutions with a zero penalty dominate obviously other solutions with non zero penalty.

All the results presented here are validated by multiple runs of the algorithm. We stop the algorithm when no visual change is noticed on the obtained sets within a period of 30 generations. The Pareto surfaces, in the objectives' space, are obtained by aggregating the sets generated by each of at least 7 runs and making a non-domination sort on the resulting set. We used the Simpson formula [21] to compute space integrals with 50 points and classical averaging to compute means in time with 100 points. We also used a value of 0.025 for $C_{m_{ref}}$ and a set of three forward velocities ($V_c = 6m/s, V_c = 10m/s, V_c = 14m/s$).

For the graphical representations, we define three adimensionalized parameters as follows :

$$\begin{aligned} DC_z^* &= \frac{C_z - C_{zc}}{C_{zc}}, \\ Eta^* &= \bar{\eta}, \\ C_m^* &= C_m / C_{m_{ref}}. \end{aligned}$$

DC_z^* can be interpreted as the ratio of the difference of the mass that can be taken by the aerial vehicle and M (0.69kg) divided by M. As we have imposed a maximal mass of $5kg$ and a minimal mass of $0.1kg$, only the solutions with a DC_z^* inferior to $DC_z^{max} = 6.5$ and superior to $DC_z^{min} = -0.85$ are feasible.

B. Dae-Kwan et al.'s model

1) The Pareto surfaces : The evolution process has found non plane Pareto surfaces for the three forward velocities, with low values of $\bar{\eta}$, between 0.02 and 0.18. We have choosen to represent the results using the scatter-plot matrix method (Fig. 10).
In the plane (Eta^*, Cm^*) (Fig. 10 (b)), we can notice that all the three sets collapse into a single curve, which shows that there is no influence of the forward velocity (within the

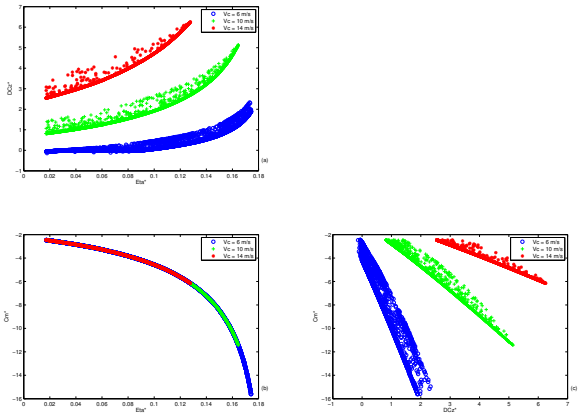

Fig. 10. Scatter-plot matrix representation for the three Pareto surfaces

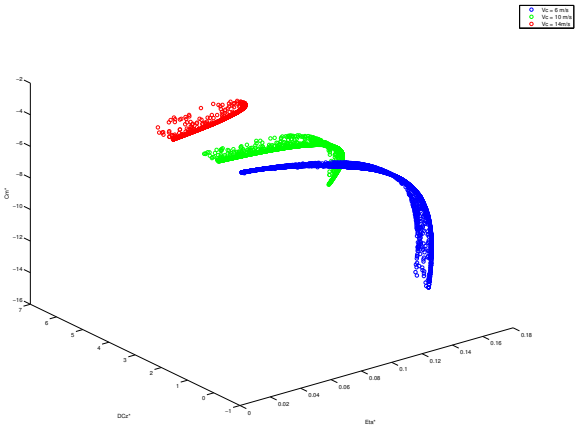

Fig. 11. The three Pareto surfaces

choosen range of velocities) on the distribution of the optimal solutions in this plane. Indeed, we can see that an increase in the propulsive effficiency is associated with an increase in the absolute value of the pitching moment which points out that efficient solutions need to be stabilized in pitch by the addition of a device (a tail for example).
Moreover, in the plane (Eta^*, DC_z^*) (Fig. 10 (a)), we can see an obvious effect of the velocity. Indeed, if we consider a given propulsive efficiency, an increase in the forward velocity leads to an increase of the DC_z^*. That means that, for this propulsive efficiency, the higher the velocity (within the choosen velocity range of course) the more additional mass the vehicle can take, which is quite compatible with the common physical sense. But we can also notice that the highest propulsive efficiency is obtained for the lowest velocity ($V_c = 6m/s$), which is quite normal because of the constraint on the DC_z^*.
Finally, in the plane (DC_z^*, Cm^*) (Fig. 10 (c)), we can see that for a given pitching moment an increase of the velocity increases the DC_z^* and that the greatest value of the absolute value for the pitching moment is obtained for the lowest velocity, which is quite normal because of the constraint on the DC_z^*. We have also included a representation of the three Pareto surfaces (Fig. 11)

As said before the solutions who have the highest propulsive efficiency are in the Pareto surface obtained at $V_c = 6m/s$ (Fig. 10). If we take a closer look at these solutions, we can notice that they are not stabilized in pitch (absolute value of Cm^* is not zero) and that they need an additional device to be stable in pitch (Fig. 12). Furthermore, we can see that they can take additional mass at this speed as the DC_z^* takes positive values.

2) The optimal parameters : Now, we are going to take a look at the optimal parameters of the dihedral harmonic motion (1). We have choosen to adopt a scatter-plot matrix representation as in section IV-B1.

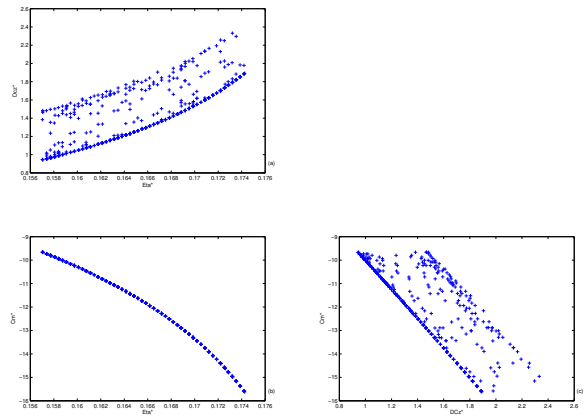

Fig. 12. Scatter-plot matrix representation for the most efficient solutions

In the plane $(d\beta, f_\beta)$ (Fig. 13 (a)), we can see that the distribution of points is symetrical with regard to the y axis. This is due to the choice of the optimization interval, which can be restricted to its half (in the comments, we will just consider the part with positive dihedral amplitude).

In addition to that, optimal frequencies (f_β) and dihedral amplitudes ($d\beta$) lie on a specific region of the plane delimited by a vertical axis of maximum dihedral amplitude, a horizontal axis of maximum frequency and a parabolic-like curve (there are two parabolic-like curves for the lowest velocity ($V_c = 6m/s$). It is worthwhile mentioning that the minima of the optimal set of frequencies and dihedral amplitudes are greater than the minimal value of the optimization interval, which means that all the frequencies and dihedral amplitudes within the optimization interval are not optimal parameters, then there is a "preference" for the frequencies higher than $3.5\ Hz$ and the dihedral amplitudes higher than $0.4\ rad$ for $V_c = 6m/s$ for example.

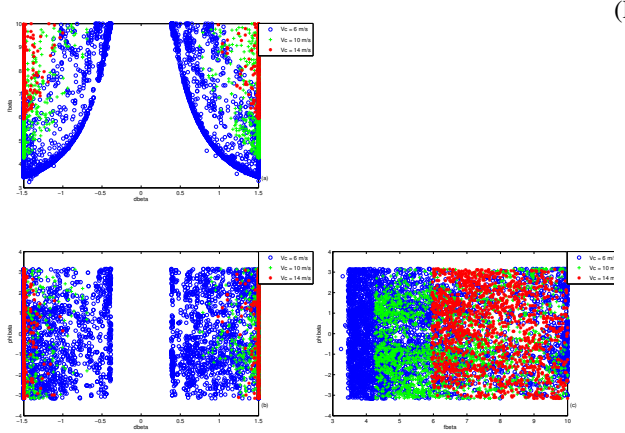

Fig. 13. Scatter-plot matrix representation for the optimal parameters of the three Pareto surfaces

Furthermore, we can see that there is a trade-off between frequency and dihedral amplitude selection for optimality. If the frequency is high, the dihedral amplitude is low and vice-versa. The velocity does not affect this "equilibrium" but increases the minimal frequencies and dihedral amplitudes and shrinks the points cloud of optimal parameters. In the planes $(d\beta, \phi_\beta)$, (f_β, ϕ_β) (Fig. 13 (b) and (c)), we can see that the phase of the dihedral motion is not a key parameter as the optimization interval choosen for the phase (ϕ_β) is uniformely populated.
Finally, we can have a look at the optimal parameters for the most efficient solutions (Fig. 14)

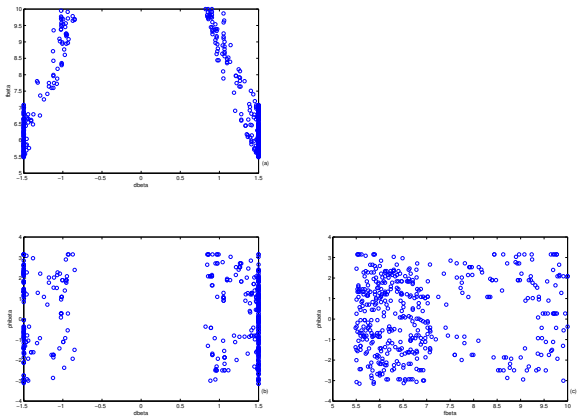

Fig. 14. Scatter-plot matrix representation for the optimal parameters of the most efficient solutions

3) Single objective computation : We have also performed a single objective computation (for the three forward velocities) by agregating the three objectives with equal weights (6,7). We have obtained feasible solutions that were not dominated by the solutions of the multiobjective computation for $V_c = 6m/s$ (Fig. 15), $V_c = 10m/s$ (Fig. 16) and $V_c = 14m/s$ (Fig. 17). One can think that our problem can be solved by

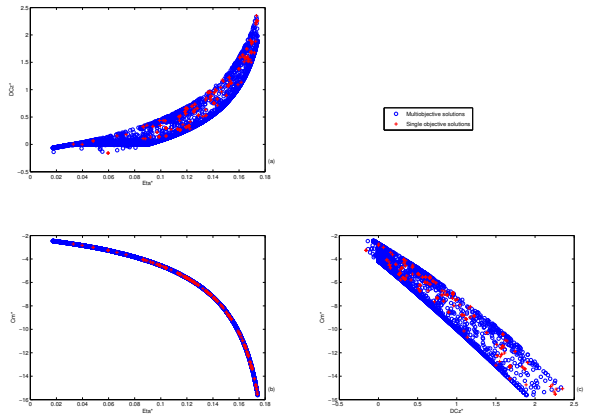

Fig. 15. Scatter-plot matrix representation of multiobjective and single objective optimal solutions for $V_c = 6m/s$

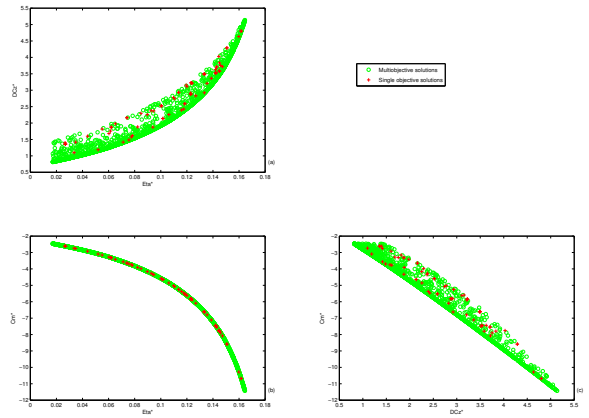

Fig. 16. Scatter-plot matrix representation of multiobjective and single objective optimal solutions for $V_c = 10m/s$

just using a single objective approach. It is not totally true. The single objective approach can give some feasible non-dominated solutions but it does not give access to the whole set of possible trade-offs (only if the Pareto surface is convex, which cannot be known in advance) among which the user can choose his solution. On the contrary, using multi-objective procedures offer the advantage of directly generating the set of the best trade-offs and then give the opportunity to have at once more choices and more insights in the structure of the problem.

C. DeLaurier's model

We performed the same optimization process with the De-Laurier's model. But the obtained sets do not contain feasible solutions. Indeed we can easily see (Fig. 18, Fig. 19) that the penalty (see IV-A) is not zero, because the objectives take values inferior to -3.0, then the solutions provided by

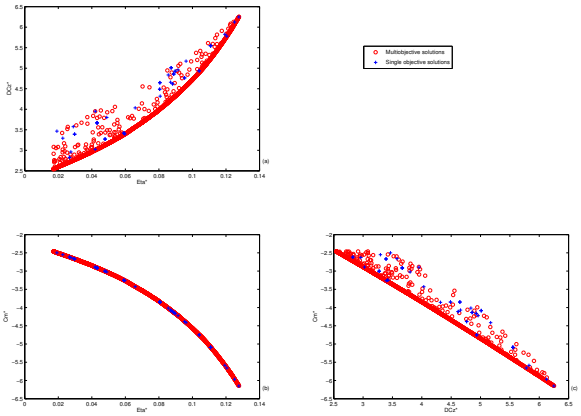

Fig. 17. Scatter-plot matrix representation of multiobjective and single objective optimal solutions for $V_c = 14m/s$

the algorithm are clearly not feasible for $V_c = 10m/s$ and $V_c = 14m/s$.

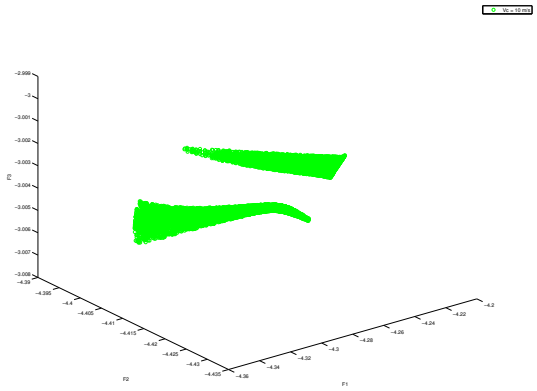

Fig. 18. Infeasible solutions obtained with DeLaurier's model for $V_c = 10m/s$

For $V_c = 6m/s$, the objectives take values between -3.0 and -1.0 (Fig. 20) but when we compute the Pareto surfaces into the physical space (Eta^*, DCz^*, Cm^*) we can easily see that the constraint on DC_z^* (DC_z^* greater than DC_z^{min}) is not respected (Fig. 21), which means that the obtained set of solutions is not feasible.

We can then conclude that the DeLaurier model is not compatible with the optimization program (OP) defined before.

V. Conclusion

In conclusion, we can say that we have performed a constrained multiobjective optimization to find optimal kinematics maximizing propulsive efficiency for a simplified birdlike aerial vehicle in horizontal motion at given speed. We used two flight physics models, Dae-Kwan *et al.* 's model and DeLaurier's model to describe the physics of the flapping wing

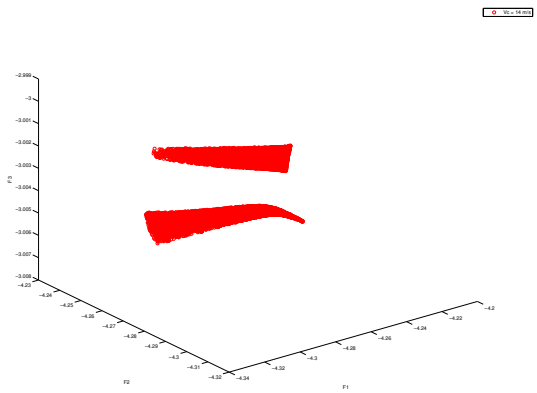

Fig. 19. Infeasible solutions obtained with DeLaurier's model for $V_c = 14m/s$

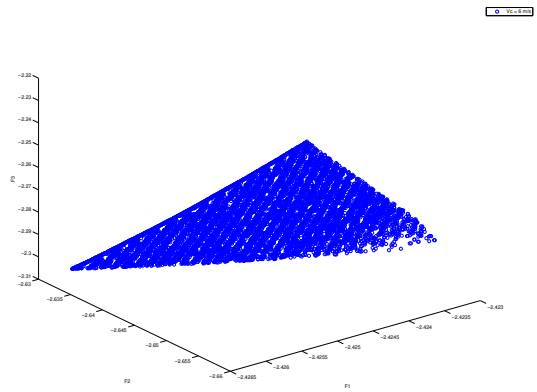

Fig. 20. Solutions obtained with DeLaurier's model for $V_c = 6m/s$

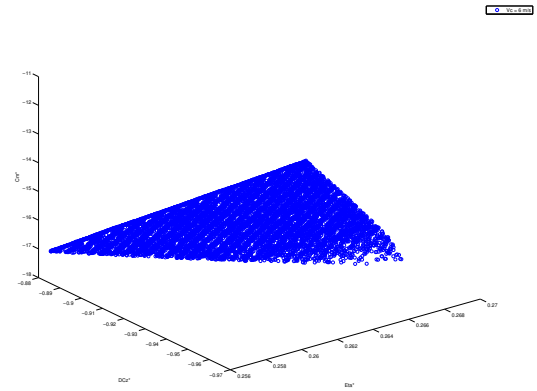

Fig. 21. Infeasible solutions obtained with DeLaurier's model for $V_c = 6m/s$

flight and evolutionary algorithms to perform the multiobjective constrained optimization.

In the case of Dae-Kwan *et al.* 's model Pareto surfaces were found. All the obtained solutions were not balanced in pitch, which means that they do need an additional device (a tail for example) to be balanced. A quick look at the optimal parameters distribution showed the existence of a trade-off between frequency and dihedral amplitude (the higher the frequency was, the lower the dihedral amplitude). The study of the change of the Pareto surfaces with the advance velocity allowed us to determine the velocity which gives the higher propulsive efficiency. In this case it is the lowest velocity ($V_c = 6m/s$).

We also launched a single objective computation a found feasible solutions that were not dominated by the multiobjective solutions. We have compared multi and single objective evolutionary algorithms. Both yields similar results, but multi-objective algorithms offer the advantage of directly generating the set of the best trade-offs between the different criteria we used for optimization instead of a single solution. Although in our experiments, the solutions generated by single objective optimization were as efficient as the one generated by multi-objective optimization, the Pareto surface gave us more insights on the structure of the search space and, consequently, on the flight models we compare and on the flight dynamics. Finally, the model proposed by DeLaurier did not yield feasible solutions, which allows us to say that it is not compatible with the optimization program (OP).

VI. Tables

TABLE I
MASS AND FREQUENCY VALUES

M_{max} (kg)	M_{min} (kg)	f_{max}(Hz)	f_{min}(Hz)
5.0	0.1	10.0	0.0

TABLE II
AERODYNAMIC PARAMETERS VALUES

$V_{max}(m.s^{-1})$	$V_{min}(m.s^{-1})$	C_{zmax}	C_{zmin}	C_{dmax}	C_{dmin}
30.00	6.00	14.3	0.01	9.92	0.10

TABLE III
OPTIMIZATION BOUNDS FOR THE KINEMATIC PARAMETERS FOR THE DIHEDRAL MOTION

	$d\beta(rad)$	$f_\beta(rad.s^{-1})$	$\phi_\beta(rad)$
Max	$\frac{\pi}{2}$	0	π
Min	$-\frac{\pi}{2}$	10	$-\pi$

TABLE IV
C_{zc} VALUES

$V_c(m.s^{-1})$	6	10	14
C_{zc}	1.97	0.71	0.36

References

[1] G. Berman and J. Wang, *Energy-minimizing kinematics in hovering insect flight*, Journal of fluid mechanics. (2007), *vol.* 582, *pp.* 153-168.

[2] Dae-Kwan Kim and Jin-Young Lee and Jun-Seong Lee and Jae-Hung Han, *An aerodynamic model of flapping-wing aircraft using modified strip theory*, Joint Intyernational Symposium, Kitakyushu, Japan,10-12.10.2007.

[3] E. de Margerie and J.-B. Mouret and J.-A. Meyer, *Artificial evolution of the morphology and kinematics in a flapping-wing mini-UAV*, Bioinspiration and Biomimetics,2 (2007) 65-82.

[4] J. W. Langelaan, *Long distance/duration trajectory optimization for small UAVs*, Guidance, Navigation and Control Conference, August 16-19 2007, South Carolina.

[5] H. Rifa, N. Marchand and G. Poulin, *OVMI - Towards a 3D-space flapping flight parametrization*, Int. Conf. on Advances in Vehicle Control and Safety, Argentina, 2007.

[6] Z. A. Khan and S K Agrawal, *Force and moment characterization of flapping wings for micro air vehicle application*, American Control Conference, June 8-10, 2006, Portland, OR, USA.

[7] S. Doncieux and J.-B. Mouret and A. Angeli and R. Barate and J.-A. Meyer and E. de Margerie, *Building an Artificial Bird: Goals and Accomplishments of the ROBUR Project*, Proceedings of the European Micro Aerial Vehicles (EMAV 2006) conference.

[8] T. Rakotomamonjy, *Analyse et contrle du vol d'un microdone ailes battantes*,*PhD Thesis*,2005.

[9] K. Deb and M. Mohan and S. Mishra, *Towards a quick computation of well-spred pareto-optimal solutions*,Proccedings of the Second Evolutionary Multi-Criterion Optimization (EMO-03) Conference, 8-11 April, Faro, Portugal.222-236.

[10] G. Pedro and A. Suleman and N. Djilali, *A numerical study of propulsive efficiency of a flapping hydrofoil*, International journal for numerical methods in fluids, 2003; **42**:493-526.

[11] J. Yan and R. J. Wood and S. Avadhanula and M. Sitti and R. S. Fearing, *Towards flapping-wing control for a micromechanical flying insect: design and experimental results*,in International Conference on robotics and Automation, Seoul.IEEE.

[12] K. Deb, *Multi-objectives optimization using evolutionnary algorithms*,*Wiley*, 2001.

[13] J. D. DeLaurier,*A nonlinear aeroelastic model for the study of flapping wing flight*,The American Institute of Aeronautics and Astronautics Inc., 2001.

[14] N. Pornsin-Siriak and Y. c. Tai and C. m. Ho and M. Keenon, *Microbat: a palm-sized electrically powered ornithopter*, in NASA/JPL Workshop on Biomorphic Robotics, Pasadena, 2001.

[15] J. Anderson, *A survey of multiobjective optimization in engineering design*, Reports of the Departement of Mechanical Engineering, LiTH-IKP-R-1097.

[16] J. D. DeLaurier,*The developpement and testing of a full-scale piloted ornithopter*,Canadian aeronautics and space journal, Vol.45, n 2, June 1999.

[17] W. Shyy, and M. berg and D. Ljungqvist,*Flapping and flexible wings for biological and micro air vehicles*, Progress in aerospace sciences 35 (1999) 455-505.

[18] J. M. Anderson and K. Streitlien and D. S. Barrett nad M. S. Triantafyllou, *Oscillating foils of high propulsive efficiency*, Journal of fluid mechanics. (1998), *vol.* 360, *pp.* 41-72.

[19] R. C. Michelson, *Update on flappi,ng wing micro air vehicle research*, in 13^{th} Bristol International RPV Conference,1998.

[20] J. D. DeLaurier, *An aerodynamic model for flapping-wing flight*,The aeronautical journal of the royal aeronautical society, April 1993.

[21] C. W. Clenshaw and A. R. Curtis, *A method for numerical integration on an automatic computer*, Numerische Mathematik 2, 197-205 (1960).

[22] K. Isoga and Y. Harino, *Optimum aeroelastic design of a flapping wing*, Journal of Aircraft,Vol. 44, 2007.

[23] M. Harada, *Calculation method for optimal circulation distribution on a finite span flapping wing* , Proceedings of the first technical conference and wokshop on unmanned aerospace vehicles, 2002.

[24] K. Miettinen, *Nonlinear Multiobjective Optimization*, Kluwer, Boston, 1999.

[25] S. Landau and S. Doncieux and A. Drogoul and J.-A. Meyer, *SFERES: un framework pour la conception de systmes multi-agents adaptatifs*, in Technique et Science Informatiques, 2002a, 21(4):427-446

Hamdaoui Mohamed Engineer of Ecole Polytechnique, Lozère, France-2006.
Engineer of ENSAE, Toulouse, France-2005.
Msc in Fluid dynamics, ENSAE, Toulouse, France-2005.
PhD student at IJLRDA, Univ. Pierre et Marie Curie - Paris 6, France, 2006-present.
His main research interests are numerical simulation in fluid dynamics and optimization with application to flapping wings aerial vehicles.

Jean-Baptiste Mouret Engineer of EPITA, Paris, France, 2004.
Msc in Artificial Intelligence, Univ. Pierre et Marie Curie - Paris 6, France, 2005.
PhD student in Artificial Intelligence at ISIR, Univ. Pierre et Marie Curie - Paris 6,France,2006-present.
His main research activities concern the optimization of neural networks for adaptive agents using multi-objective evolutionary algorithms.

Stéphane Doncieux Engineer of ENSEA, cergy-Pontoise, France, 1996-1999.
Msc in Artificial Intelligence (Pattern recognition and applications), Univ. Pierre et Marie Curie - Paris 6,France, 1998-1999.
PhD in Artificial Intelligence, Univ. Pierre et Marie Curie - Paris 6,France,1999-2003.
Lecturer at Univ. Pierre et Marie Curie - Paris 6, France,2004-present.
He is currently coordinator of SIMA research team (Integrated, Mobile and Autonomous Systems) and he is in charge of the ROBUR project, which aims at building an autonomous flapping wing robot. Its research activities deal with evolutionary robotics and more generally autonomous robots.

Pierre Sagaut Msc in Fluid mechanics Univ. Pierre et Marie Curie - Paris 6,France, 1991.
PhD in Fluid Mechanics, Univ. Pierre et Marie Curie - Paris 6,France, 1995.
Senior scientist at ONERA (CFD and Acoustics Dept.) France, 1995-2002.
Professor, (Mechanical Engng. Dept.), Univ. Pierre et Marie Curie - Paris 6, 2002-present.
Publications, 100 articles in international journals, 6 monographs. Awards and prizes, John Green Prize (2002), EREA award (2007, with E. Manoha and G. Desquesnes).
Editorial board membership : Theoretical and Computational Fluid Dynamics, Progress in CFD, Journal of Scientific Computing, Springer's Scientific Computation Series.